12th International Symposium on Turbulence and Shear Flow Phenomena (TSFP12)
Osaka, Japan (Online), July 19-22, 2022

ASSESSMENT OF OUTER-LAYER SIMILARITY IN TURBULENT FLOWS OVER CANOPIES

Zishen Chen
Department of Engineering
University of Cambridge
Trumpington Street, Cambridge, CB2 1PZ, UK
zc328@cam.ac.uk

Ricardo García-Mayoral
Department of Engineering
University of Cambridge
Trumpington Street, Cambridge, CB2 1PZ, UK
r.gmayoral@eng.cam.ac.uk

ABSTRACT

Turbulent flows over rough and complex surfaces generally exhibit a similar character to those over smooth walls sufficiently far above the surface (Townsend, 1976). The inner length and velocity scales for these flows are typically evaluated at the reference height, $y_* = 0$, used as the virtual origin to obtain a smooth-wall-like logarithmic layer. However, recent studies have reported the loss of this outer-layer similarity in turbulence over highly obstructing layouts, such as canopies and permeable substrates (Okazaki *et al.*, 2021; Manes *et al.*, 2011). In this study, we probe the existence of outer-layer similarity for a series of direct numerical simulations of canopies of varying density. By the assessment of the diagnostic function of the mean velocity profile, it is shown that as canopy density decreases, the overlying turbulent flow perceives a deeper virtual origin into the canopy. Based on the length and velocity scales provided by the virtual origin, the turbulent flow over the densest canopy with $\lambda_f \approx 2.04$ is essentially smooth-wall-like. However, canopies with $\lambda_f \approx 0.01 - 0.91$ result in values of Kármán constant, $\kappa \approx 0.34 - 0.43$, different from the smooth-wall value, $\kappa \approx 0.4$, while turbulent statistics are essentially smooth-wall-like in the logarithmic layer and above. This suggests a modified outer-layer similarity where κ is not 0.4, but otherwise the canopy flows are outer-layer similar to a smooth-wall flow.

Introduction

Turbulent boundary layers over rough and complex surfaces are ubiquitous and are of significant environmental and industrial interest (Jiménez, 2004; Finnigan, 2000). Studies of wall-bounded turbulence have provide the tools for understanding these rough-wall flows, with engineering models that treat roughness as a small perturbation to the smooth-wall boundary layer (Flack *et al.*, 2007; Wu & Christensen, 2007). However, if the roughness-induced perturbation propagates into the outer layer, the scaling based on smooth-wall similarity could produce erroneous results. Understanding the extent of roughness effects and whether this smooth-wall similarity holds true is therefore of great importance to various applications.

The surface topology has a direct impact on the flow within the 'roughness sublayer,' which can extend up to $2-3$ roughness heights or spacings above the roughness crests, depending on the density regime (Jiménez, 2004; Brunet, 2020). Above this height, it is widely accepted that the turbulence is essentially undisturbed and exhibits outer-layer similarity (Clauser, 1954; Townsend, 1976). The only effect is then a constant shift, ΔU^+, in the mean velocity profile, while both the Kármán constant, $\kappa \approx 0.4$, and the 'wake' region are unaffected. Townsend (1976) proposed the outer-layer similarity hypothesis, articulating that at a sufficiently high Reynolds number, the turbulent eddies in the outer layer would be essentially unaffected by the surface topology. The surface affects the flow only through providing the relevant scales, the wall shear stress, τ_w, or the friction velocity, $u_\tau = (\tau_w/\rho)^{1/2}$, and the characteristic length scale provided by the distance to the wall, y. However, whether surface effects extend beyond the 'roughness sublayer' and into the outer layer is still a topic of debate as conflicting evidence exists for some surfaces (Wu & Christensen, 2007; Flack & Schultz, 2010). Experimental and numerical studies for turbulent flows over porous media carried out by Breugem *et al.* (2006), Suga *et al.* (2010), Manes *et al.* (2011), and Okazaki *et al.* (2021) have reported the loss of outer-layer similarity and values for κ very different from $\kappa \approx 0.4$ at $Re_\tau \approx 400 - 5800$, suggesting a more in-depth modification of the flow by the substrates.

The canonical logarithmic form of the mean velocity profile for a turbulent flow is

$$U^+ = \frac{1}{\kappa}\log(y^+ - \Delta y^+) + A - \Delta U^+, \tag{1}$$

where κ is the Kármán constant and $\kappa \approx 0.4$ if outer-layer similarity recovers, A is the log-law intercept for a smooth-wall flow, ΔU^+ is the velocity deficit caused by the substrate, and Δy^+ is the zero-plane displacement that recovers outer-layer similarity for the mean velocity profile, U^+. However, recent studies suggest that the scaling for wall turbulence is essentially local, and is given by the local mean shear and pro-

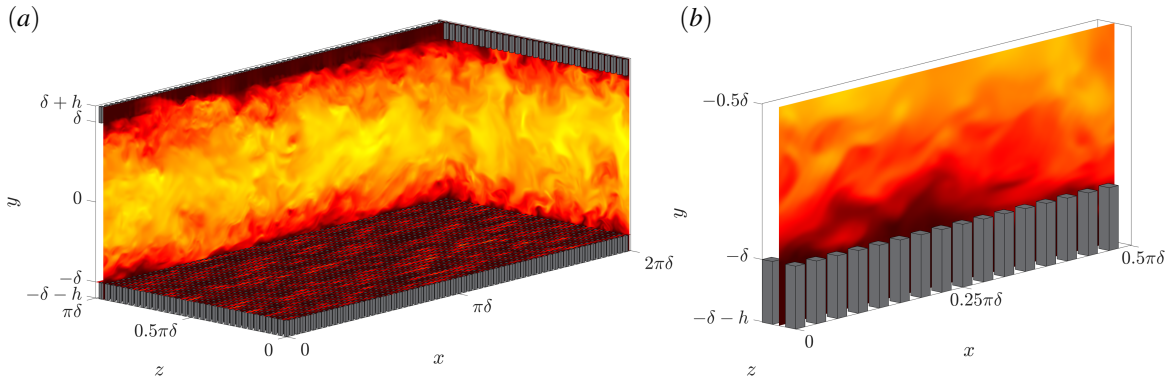

Figure 1. Schematics of (a) the numerical domain and (b) a zoomed cross-section for case D54. An instantaneous realisation of the streamwise velocity is shown in the orthogonal planes.

duction rate of turbulent kinetic energy, with no explicit reference to the wall-normal distance (Lozano-Durán & Bae, 2019; Tuerke & Jiménez, 2013). This implies that the traditional scaling based on y and u_τ happens to hold because of the one-to-one correspondence between them and the local production and shear, but this correspondence does not need to hold necessarily for every flow. As part of this work, we have investigated, for flows that exhibit an apparent loss of outer-layer similarity, whether the local scale can still have correspondence to a friction velocity, $u_\tau^\star$, and a length scale, y_* where y_* is zero at the height of zero-plane displacement, but $u_\tau^\star$ is not necessarily evaluated at $y_* = 0$. Here, superscript $(\cdot)^\star$ denotes wall units defined by ν and $u_\tau^\star$ decoupled from $y_* = 0$, and superscript $(\cdot)^*$ denotes wall units defined by ν and u_τ^* evaluated at $y_* = 0$. Subscript $(\cdot)_*$ denotes outer units that are normalised by the bulk velocity and outer length scale, y_*, measured from the virtual origin.

The diagnostic function of the mean velocity profile is (Luchini, 2018)

$$\beta(y_*^+) = y_*^+ \frac{\partial U^+}{\partial y_*^+}, \tag{2}$$

where $y_*^+ = (y - \Delta y)^+$ is the wall-normal distance from the virtual origin at $y_* = 0$, which would exhibit a plateau $\beta \approx 1/\kappa$ in the logarithmic layer, if outer-layer similarity recovered. Many previous studies rely on the existence of this plateau to determine the extent of the logarithmic layer and the inner scaling in flows over roughness (Suga *et al.*, 2010; Breugem *et al.*, 2006). Particularly, the logarithmic law in Eq.(1) can be recovered by choosing a Δy that yields a plateau in $(y - \Delta y)dU/dy$ with value u_τ^*/κ. The inner velocity and length scales are then determined based on u_τ^* evaluated at the reference height, $y_* = 0$. However, a logarithmic layer with a plateau in β emerges only in a flow at high Re_τ. According to numerical evidence, $Re_\tau \approx 5200$ is not yet high enough for the diagnostic function of a wall-bounded turbulent flow to exhibit a completely flat plateau (Lee & Moser, 2015; Yamamoto & Tsuji, 2018; Luchini, 2018). Additionally, outer-layer similarity, by definition, refers to the similarity in not just the logarithmic layer but also the 'wake' region. For a flow at limited Re_τ, neglecting similarity in the 'wake' region while enforcing a plateau in the diagnostic function could therefore result in erroneous predictions of parameters including Δy, u_τ^*, and κ .

In this study, we determine the zero-plane displacement, Δy, by minimising the deviation of the diagnostic function in the logarithmic layer and above, compared to that of a smooth-wall flow at roughly the same Re_τ. We assess the validity as a scaling velocity of the friction velocity both measured at the height of zero-plane displacement and set as an independent, free parameter. With this, we probe the existence of outer-layer similarity in turbulence over canopies of varying density.

Table 1. Simulation parameters: $Re_\tau = u_\tau \delta/\nu$ is the friction Reynolds number based on $\delta = 1$, the half-channel height, u_τ calculated from the total shear at the canopy tips, and kinematic viscosity, ν; λ_f is the frontal density; h and s are the canopy height and streamwise and spanwise spacing; Δ_x^+ and Δ_z^+ are the streamwise and spanwise resolutions; $\Delta_{y,f}^+$ and $\Delta_{y,t}^+$ are the wall-normal resolutions at the floor and canopy tips.

Case	Re_τ	λ_f	s/h	Δ_x^+	Δ_z^+	$\Delta_{y,f}^+$	$\Delta_{y,t}^+$
S	550.6	-	-	9.01	4.50	0.27	-
D36	550.3	2.04	0.33	2.00	2.00	2.95	0.5
D54	550.1	0.91	0.49	3.00	3.00	2.53	0.50
I72	551.9	0.51	0.65	4.01	4.01	2.01	1.00
I108	548.5	0.23	0.98	5.98	2.99	2.00	1.00
I144	547.0	0.13	1.31	5.97	2.98	1.19	1.19
S216	549.0	0.06	1.96	5.99	2.99	1.00	1.00
S288	547.9	0.03	2.62	5.98	2.99	0.79	0.79
S432	548.9	0.01	3.93	5.99	2.99	0.60	0.60

Direct Numerical Simulations

We carry out a series of direct numerical simulations (DNSs) of closed channels with canopies of rigid filaments covering the walls at moderate Reynolds numbers ($Re_\tau \approx 550$). The size of the numerical domain is $L_x \times L_z \times L_y = 2\pi\delta \times \pi\delta \times 2(\delta + h)$, where δ is the half-channel height and h is the canopy height. We vary the canopy density by changing the spacing between elements, resulting in frontal densities, $\lambda_f \approx 0.01 - 2.04$ (Nepf, 2012; Sharma & García-Mayoral, 2020*a*,*b*). All canopies considered consist of collocated prismatic posts with sides $l_x^+ = l_z^+ \approx 24$ and height $h^+ \approx 110$, as depicted in Figure 1. Relevant simulation parameters are listed in Table1. Case S is a reference smooth-wall channel. For the canopy simulations, letters 'D', 'I', and 'S' denote dense, intermediate, and sparse configurations (Nepf, 2012; Brunet, 2020), and the number that follows denotes the approximate spacing, s^+, between the canopy elements.

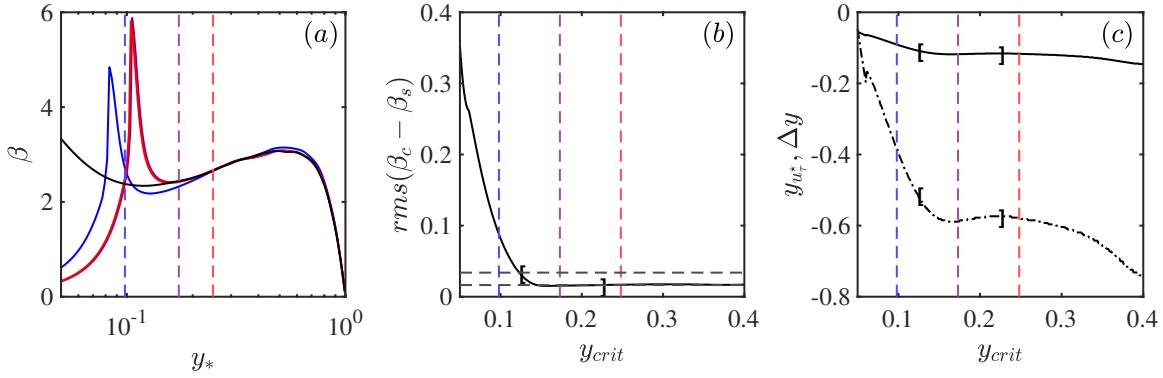

Figure 2. (a) Canopy diagnostics function for case I144 scaled with y_* and $u_\tau^\star$ that minimise the r.m.s. deviation from the smooth-wall profile above a critical height. ——, smooth-wall statistics at $Re_\tau \approx 550$; ——, ——, ——, canopy statistics based on - - -, $y_{crit} = 0.098$; - - -, $y_{crit} = 0.173$; - - -, $y_{crit} = 0.248$. The wall-normal coordinate for the shifted profiles is $y_* = (y - \Delta y)/(1 - \Delta y)$. (b) ——, r.m.s. deviation between β_s and β_c; - - -, once and twice the baseline error; [and], bounds for y_{crit}. (c) ——, zero-plane displacement, Δy; - · - ·, height where $u_\tau^\star$ is evaluated at, $y_{u_\tau^\star}$.

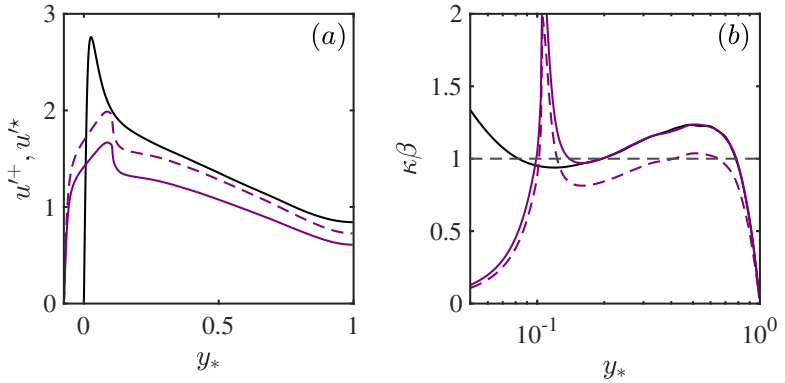

Figure 3. (a) Streamwise r.m.s. velocity fluctuation for case I144 scaled with - - -, u_τ^* and ——, $u_\tau^\star$ based on $y_{crit} = 0.173$. (b) Logarithmic relationship in Eq.(3) - - -, $\kappa_c \cdot y^\star \partial U^\star / \partial y_*$; ——, $\kappa_c \cdot y^+ \partial U^+ / \partial y_*^+$; - - -, $\kappa_s \beta_s = 1$. In (a) and (b), ——, smooth-wall reference statistics at $Re_\tau \approx 550$.

The simulations solve the three-dimensional incompressible turbulent flow in a symmetric channel with rigid canopy elements attached to both walls, as portrayed in Figure 1. No-slip and no-penetration boundary conditions are enforced at both walls. The canopy elements are explicitly resolved using a direct-forcing, immersed-boundary method (García-Mayoral & Jiménez, 2011). The domain is periodic in the wall-parallel directions (x, z), which are discretised spectrally. A second-order central difference scheme on a staggered grid is used in the wall-normal direction (y), for which the grid is stretched with $\Delta_y^+ \approx 4.5$ at the channel centre. The wall-normal grid resolutions at the floor and the canopy tips, where mean shear concentrates, are listed in Table 1. The temporal discretisation uses a semi-implicit Runge-Kutta, fractional-step method (Le & Moin, 1991), and the channel is driven by a constant mean pressure gradient, with viscosity adjusted to obtain $Re_\tau \approx 550$. Each simulation is run for at least 10 largest eddy-turnover times, δ/u_τ, to wash out any initial transients. Once the flow reaches a statistically steady state, statistics are collected over 10-15 δ/u_τ. Full details of the numerical method can be found in Sharma & García-Mayoral (2020*a*,*b*).

Results and Discussion

Because the surface morphology has a direct impact on the flow within the 'roughness sublayer', of thickness y_{crit}, we expect no outer-layer similarity below $y_* = y_{crit}$. To determine Δy and $u_\tau^\star$ that recover a smooth-wall-like β_c, we therefore minimise the deviation between β_s and β_c, the smooth-wall and canopy diagnostic functions, above y_{crit}. Additionally, because y_{crit} can vary depending on the canopy density regime, y_{crit} need to be determined separately for each canopy flow, (Jiménez, 2004; Brunet, 2020). By this method, we avoid enforcing a plateau in β_c artificially, relying on just the logarithmic layer. Instead, we recover a smooth-wall-like β_c in the logarithmic layer and above.

We first assess the sensitivity of the results to the choice of y_{crit}. As an example, Figure 2(a) depicts the diagnostic function of case I144 for different values of y_{crit}. For $y_{crit} = 0.098$, β_c is not smooth-wall-like above this height even if the deviation between β_s and β_c is minimised. This is because y_{crit} is so small that the flow just above y_{crit} is still within the 'roughness sublayer' and is perturbed by the canopy elements. However, for $y_{crit} \geq 0.173$, β_c is smooth-wall-like for all y_* greater than y_{crit}. As shown in Figure 2(b), the r.m.s. deviation between β_c and β_s remains stable and small when $y_{crit} \geq 0.173$. Nevertheless, the deviation between β_c and β_s persists even for large y_{crit}. The major source of this persistent deviation may be attributed to the numerical noise in β_s and β_c, as depicted in Figure 2(a).

In the above, we have left the friction velocity as an independent parameter. To determine Δy and $u_\tau^\star$, which are functions of y_{crit} as depicted in Figure 2(c), we need to set the lower and upper bounds for y_{crit}. In Figure 2(b), the lower

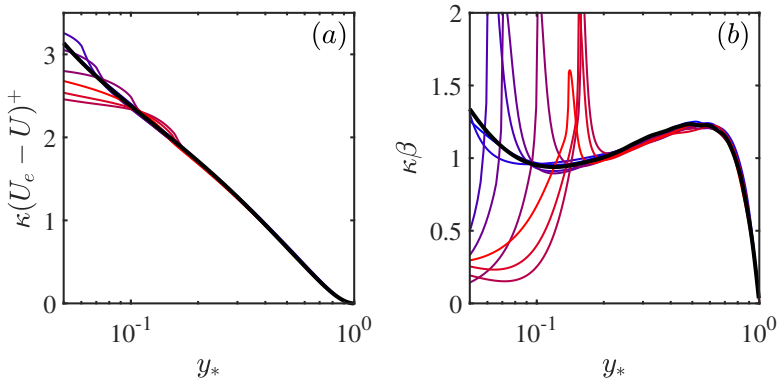

Figure 4. (a) Modified defect-law velocity profiles and (b) modified diagnostic functions, $\kappa \cdot y_*^+ \partial U^+/\partial y_*^+$, scaled with the friction velocity, u_τ^*, evaluated at the virtual origins, as shown in Figure 7. ——, smooth-wall reference statistics; ——to ——, dense to sparse canopy statistics.

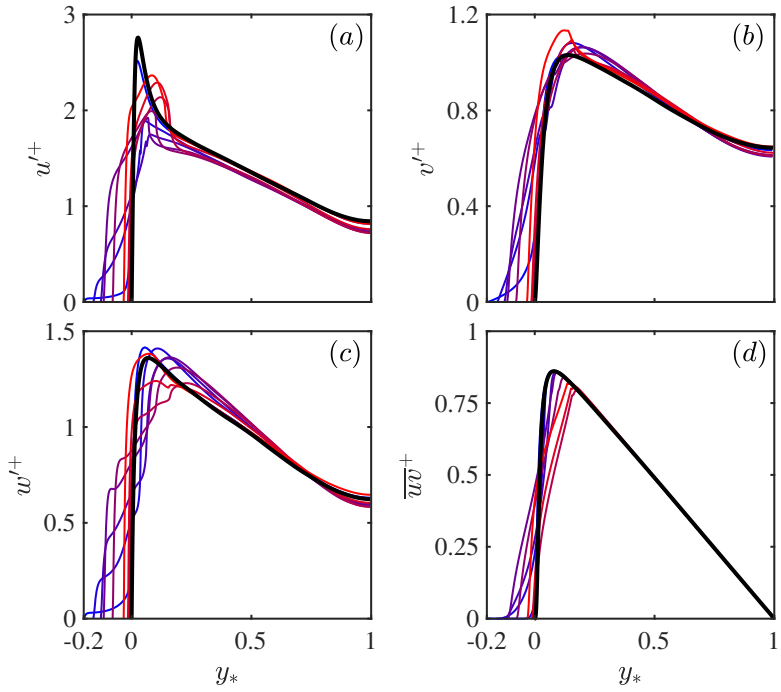

Figure 5. Turbulent r.m.s velocity fluctuations of smooth-wall and canopy flows scaled with the friction velocity, u_τ^*, evaluated at the virtual origins, as shown in Figure 7. The colour scheme is as in Figure 4.

bound for y_{crit} is given by the intersection between the r.m.s. error curve and twice the baseline error—the r.m.s. $\beta_c - \beta_s$ when y_{crit} is large. Above this lower bound, the deviation between β_c and β_s is small, and a smooth-wall-like β_c can be recovered based on Δy and $u_\tau^\star$ obtained from all y_{crit} above the lower bound. We set the upper bound 0.1 above the lower bound, as the r.m.s. $\beta_c - \beta_s$ varies little beyond this.

As shown in Figure 2, the critical height where outer-layer similarity recovers for I144 is $y_{crit} = 0.173 \pm 0.05$, which is smaller than the typical roughness layer thickness (1-2h above the canopy tips). Additionally, because y_{crit}/δ is smaller than the typical upper bound for the logarithmic region ($y \approx 0.3\delta$), we expect the recovery of a smooth-wall-like logarithmic layer for the canopy flow (Luchini, 2018; Yamamoto & Tsuji, 2018). Based on the confidence interval of y_{crit}, we obtain the zero-plane displacement, $\Delta y = -0.113 \pm 0.005$, and the height where $u_\tau^\star$ is evaluated at, $y_{u_\tau^\star} = -0.574 \pm 0.063$—note that $y_{u_\tau^\star} \neq \Delta y$.

Despite y_* and $u_\tau^\star$ yielding a smooth-wall-like β_c, the turbulent velocity fluctuations are better scaled by u_τ^* than by $u_\tau^\star$, as illustrated in Figure 3(a). Alternatively, the diagnostic function can be shown to exhibit the same smooth-wall-like behaviour if, rather than setting the friction velocity independently of the zero-plane displacement height, κ is allowed to be different from its smooth-wall value, as shown in Figure 3(b). In the logarithmic layer, Eq.(2) can be expressed as

$$\kappa_c y_*^+ \frac{\partial U^+}{\partial y_*^+} = 1, \kappa_c = (u_\tau^*/u_\tau^\star)\kappa_s, \tag{3}$$

where $\kappa_s \approx 0.4$ is the smooth-wall Kármán constant, and κ_c is the new canopy-flow Kármán constant.

Both the diagnostic function, $\kappa_c \beta_c$, and the defect law for κU^+ exhibit a good collapse with smooth-wall data, as shown in Figure 4. This implies the recovery of a logarithmic layer, but with a Kármán constant different from $\kappa_s \approx 0.4$. Figures 5 and 6 show that the turbulent velocity fluctuations and Reynolds shear stress are significantly perturbed by the presence of the canopy in the near-wall region, $y_* \lesssim 0.2$, while in

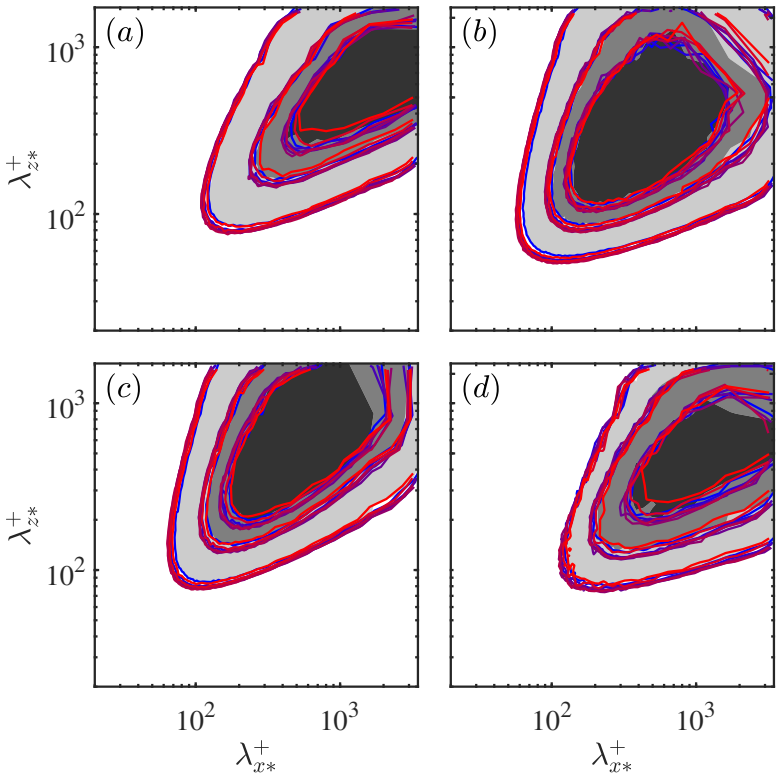

Figure 6. Pre-multiplied spectral energy densities at $y_* = 0.5\delta$ for the smooth-wall (filled contours) and canopy flows (line contours): (a) $k_x k_z E_{uu}$; (b) $k_x k_z E_{vv}$; (c) $k_x k_z E_{ww}$; (d) $k_x k_z E_{uv}$. The contours in $(a-c)$ are at 0.1, 0.3 and 0.5 times the maximum level. The contours in (d) are at 0.05, 0.2 and 0.5 times the maximum level. The colour scheme is as in Figure 4.

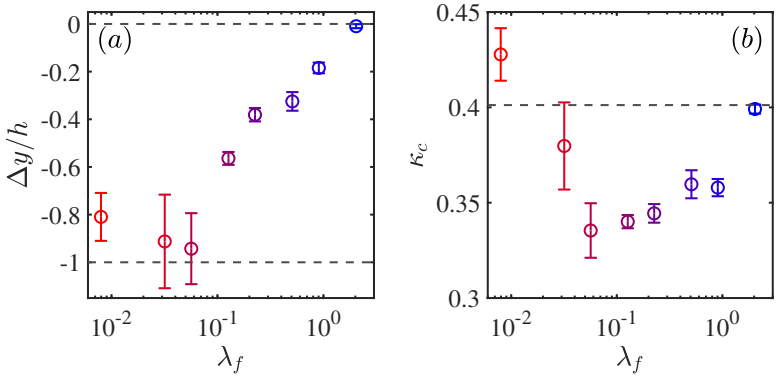

Figure 7. (a) Ratio of zero-plane displacement to canopy height, $\Delta y/h$, and (b) canopy-flow Kármán constant, κ_c. In (a), - - -, canopy-tip plane, $y/h = 0$, and floor, $y/h = -1$. In (b), - - -, smooth-wall Kármán constant, $\kappa_s \approx 0.4$, obtained from the logarithmic layer, $y^+ = 80$ to $y = 0.25\delta$. The colour scheme is as in Figure 4.

the outer layer, $y_* \gtrsim 0.3$, they are essentially smooth-wall-like.

The ratio of zero-plane displacement to canopy height, $\Delta y/h$, and the Kármán constant, κ_c, for each canopy flow are portrayed in Figure 7. For the densest canopy, with $\lambda_f \approx 2.04$, Δy is essentially zero, and $\kappa_c \approx 0.4$, suggesting that the overlying turbulence is essentially smooth-wall-like and perceives a virtual origin at the canopy-tip plane. Scaling with the friction velocity evaluated at the canopy tips has also been reported in the study of turbulence over dense filament canopies by Sharma & García-Mayoral (2020*b*). In the densest canopies investigated, the turbulent flow 'skimmed' over the canopy tips, as the turbulent eddies were precluded from penetrating within and interacting with the canopy elements, to the point that the flow above the canopy-tip plane resembles a smooth-wall flow (Brunet, 2020). However, canopies with $\lambda_f \approx 0.01 - 0.91$ have κ_c values very different from that of a smooth-wall flow, as depicted in Figure 7(b), implying a deeper modification of the flow by the presence of the canopy.

The zero-plane displacement, Δy, is associated with the depth that shear can penetrate within a porous media (Jackson, 1981; Clifton *et al.*, 2008), and this shear penetration depth increases with permeability (Okazaki *et al.*, 2021). This trend is depicted in Figure 7(a). As canopy density decreases, the outer-layer flow perceives a deeper virtual origin, and for the sparse cases with $\lambda_f \approx 0.01 - 0.06$, the virtual origins are very close to the floor. However, for the intermediate to dense cases with $\lambda_f \approx 0.51 - 2.04$, $\Delta y/h$ is small because the closely-packed canopy elements obstruct the shear penetration. Figure 7(b) indicates that cases with $\lambda_f \approx 0.03 - 0.91$ exhibit κ_c smaller than $\kappa_s \approx 0.4$. We note that $\kappa_c < 0.4$ is also observed by studies that enforce a plateau in $(y - \Delta y)^+ dU^+/dy^+$ (Breugem *et al.*, 2006; Suga *et al.*, 2010). However, the spars-

est canopy, with $\lambda_f \approx 0.01$, results in $\kappa_c > \kappa_s \approx 0.4$, which to the best of the authors' knowledge has not been reported by any previous studies.

Conclusions

In the present work, we have assessed outer-layer similarity in flows over canopies with various λ_f. To obtain the zero-plane displacement that recovers a smooth-wall-like diagnostic function, we minimise its deviation from smooth-wall results above the 'roughness sublayer,' instead of merely enforcing a plateau in the logarithmic layer. We do so because a plateau in β equal to $1/\kappa$ emerges only at high Re_τ, and also because we obtain a smooth-wall-like β not only in the logarithmic layer but also in the 'wake' region. However, an independently set friction velocity results in poor scaling for the turbulent fluctuations, so we measure the friction velocity at the height of zero-plane displacement, which leads to a Kármán constant different from $\kappa_s \approx 0.4$. When scaled with u_τ^* and y_*, the turbulent fluctuations, velocity profile and diagnostic function are similar to those of a smooth-wall flow, indicating the recovery of outer-layer similarity, but with a Kármán constant different from $\kappa_s \approx 0.4$. As the canopy density decreases, the outer-layer flow perceives a deeper virtual origin. For the sparsest cases, the virtual origins are close to the floor, indicating a significant flow penetration into the canopy. For intermediate densities, the Kármán constant is smaller than $\kappa_s \approx 0.4$, which is consistent with results from previous studies on outer-layer similarity (Breugem *et al.*, 2006; Suga *et al.*, 2010). For our sparsest canopy, κ_c is larger than $\kappa_s \approx 0.4$.

Acknowledgements

Computational resources were provided by the 'Cambridge Service for Data Driven Discovery' operated by the University of Cambridge Research Computing Service through EPSRC Tier-2 grant EP/P020259/1 and by the 'ARCHER2' system through PRACE project pr1u1702-ESTONT.

REFERENCES

Breugem, W. P., Boersma, B. J. & Uittenbogaard, R. E. 2006 The influence of wall permeability on turbulent channel flow. *Journal of Fluid Mechanics* **562**, 35–72.

Brunet, Yves 2020 Turbulent Flow in Plant Canopies: Historical Perspective and Overview. *Boundary-Layer Meteorology* **177** (2), 315–364.

Clauser, Francis H. 1954 Turbulent Boundary Layers in Adverse Pressure Gradients. *Journal of the Aeronautical Sciences* **21** (2), 91–108.

Clifton, Andrew, Manes, Costantino, Rüedi, Jean-Daniel, Guala, Michele & Lehning, Michael 2008 On shear-driven ventilation of snow. *Boundary-Layer Meteorology* pp. 249–261.

Finnigan, John 2000 Turbulence in plant canopies. *Annual Review of Fluid Mechanics* **32** (1), 519–571.

Flack, Karen A. & Schultz, Michael P. 2010 Review of Hydraulic Roughness Scales in the Fully Rough Regime. *Journal of Fluids Engineering* **132** (4).

Flack, K. A., Schultz, M. P. & Connelly, J. S. 2007 Examination of a critical roughness height for outer layer similarity. *Physics of Fluids* **19** (9), 095104.

García-Mayoral, Ricardo & Jiménez, Javier 2011 Hydrodynamic stability and breakdown of the viscous regime over riblets. *Journal of Fluid Mechanics* **678**, 317–347.

Jackson, P. S. 1981 On the displacement height in the logarithmic velocity profile. *Journal of Fluid Mechanics* **111**, 15–25.

Jiménez, Javier 2004 Turbulent flows over rough walls. *Annual Review of Fluid Mechanics* **36** (1), 173–196.

Le, Hung & Moin, Parviz 1991 An improvement of fractional step methods for the incompressible Navier-Stokes equations. *Journal of Computational Physics* **92** (2), 369–379.

Lee, Myoungkyu & Moser, Robert D. 2015 Direct numerical simulation of turbulent channel flow up to $Re_\tau \approx 5200$. *Journal of Fluid Mechanics* **774**, 395–415.

Lozano-Durán, Adrián & Bae, Hyunji Jane 2019 Characteristic scales of Townsend's wall-attached eddies. *Journal of Fluid Mechanics* **868**, 698–725.

Luchini, Paolo 2018 Structure and interpolation of the turbulent velocity profile in parallel flow. *European Journal of Mechanics - B/Fluids* **71**, 15–34.

Manes, C., Poggi, D. & Ridolfi, L. 2011 Turbulent boundary layers over permeable walls: scaling and near-wall structure. *Journal of Fluid Mechanics* **687**, 141–170.

Nepf, Heidi M. 2012 Flow and transport in regions with aquatic vegetation. *Annual Review of Fluid Mechanics* **44** (1), 123–142.

Okazaki, Yuki, Takase, Yumeto, Kuwata, Yusuke & Suga, Kazuhiko 2021 Describing characteristic parameters of turbulence over two-dimensional porous roughness. *Journal of Thermal Science and Technology* **16** (2), JTST0027–JTST0027.

Sharma, Akshath & García-Mayoral, Ricardo 2020*a* Scaling and dynamics of turbulence over sparse canopies. *Journal of Fluid Mechanics* **888**.

Sharma, Akshath & García-Mayoral, Ricardo 2020*b* Turbulent flows over dense filament canopies. *Journal of Fluid Mechanics* **888**.

Suga, K., Matsumura, Y., Ashitaka, Y., Tominaga, S. & Kaneda, M. 2010 Effects of wall permeability on turbulence. *International Journal of Heat and Fluid Flow* **31** (6), 974–984.

Townsend, A. A. R. 1976 *The Structure of Turbulent Shear Flow*. Cambridge University Press.

Tuerke, Florian & Jiménez, Javier 2013 Simulations of turbulent channels with prescribed velocity profiles. *Journal of Fluid Mechanics* **723**, 587–603.

Wu, Y. & Christensen, K. T. 2007 Outer-layer similarity in the presence of a practical rough-wall topography. *Physics of Fluids* **19** (8), 085108.

Yamamoto, Yoshinobu & Tsuji, Yoshiyuki 2018 Numerical evidence of logarithmic regions in channel flow at $\mathrm{Re}_\tau = 8000$. *Phys. Rev. Fluids* **3**, 012602.